ELSEVIER

European Journal of Pharmaceutics and Biopharmaceutics 49 (2000) 1–9

European Journal of Pharmaceutics and Biopharmaceutics

www.elsevier.com/locate/ejphabio

Research paper

Characterization of microcapsules by confocal laser scanning microscopy: structure, capsule wall composition and encapsulation rate

A. Lamprecht, U.F. Schäfer, C.-M. Lehr*

Department of Biopharmaceutics and Pharmaceutical Technology, Saarland University, Saarbrücken, Germany

Received 3 June 1999; accepted in revised form 16 September 1999

Abstract

The potential of confocal laser scanning microscope (CLSM) has been evaluated for characterizing microcapsules. The aim was to visualize the polymer distribution within the particle wall, and to localize and to quantify the encapsulated oil phase. Microcapsules were prepared by complex coacervation: the oil phase, gelatine, and arabic gum were labelled with fluorescent markers. For all compounds it was proved that fluorescence labelling did not alter physico-chemical properties critical to the encapsulation process. Labelling of the inner oil phase allowed us to identify and to localize, three-dimensionally, the encapsulated compound. A homogeneous distribution for both gelatine and arabic gum throughout the capsule wall was observed. The addition of fluorescently labelled casein as a macromolecular model compound to the coacervate resulted in an inhomogeneous distribution of casein within the wall material, the highest concentration of casein was found at the oil–wall interface. To determine the encapsulation rate, CLSM pictures of the microcapsule samples were acquired using different fluorescence labels for the microcapsule wall polymers and the incorporated oil phase, respectively. By applying computational image analysis, the volumes of the different phases were calculated. Comparing the results of non-destructive image analysis with those obtained by degradation, extraction and chemical analysis, a linear relation was found with correlation coefficients better than 0.980.

Keywords: Confocal laser scanning microscopy; Microcapsules; Microencapsulation; Complex coacervation; Polymer

1. Introduction

The complex coacervation process is a well established method for the microencapsulation of oils or solids [1–4]. Especially in the food industry this method is used to mask a potentially bad taste or to avoid oxidation of the incorporated material, e.g. certain vitamins and/or unsaturated fatty acids. Complex coacervation is one of the few methods which can be applied to natural polymers [5], one of the most important prerequisites for the processing of food supplements.

For many reasons it is of interest to analyse and to visualize the encapsulated oil phase or the deposition/distribution of the involved polymers. Commonly used visualization techniques for microparticles and microcapsules include conventional light microscopy (LM) and scanning electron microscopy (SEM) [6–9]. LM is always impeded by the scattered or emitted light from structures outside the optical focal plane. SEM, in contrast, usually requires a relatively complex sample pre-treatment (e.g. gold sputtering, etc.) and does not allow visualization of the inner structures of objects. Mechanical sections of embedded particles allow inspection of the particle wall structure, but it is not possible to visualize the encapsulated phase which is often lost during the microscopy sample pre-treatment.

In confocal laser scanning microscopy (CLSM) the light from out-of-focus structures is faded out, and at the same time this technique enables a non-destructive view through the capsule wall, provided the material is sufficiently translucent. By using different fluorescence labels, the unambiguous identification of several compounds is possible. By collecting several coplanar cross sections, a three-dimensional reconstruction of the inspected objects can be performed. Hence, computational image analysis allows the visualization and quantification of structures not only on the surface, but also inside the material.

The aim of this study was to examine the potential advantages of CLSM as a new tool for the characterization of microcapsules. First, we were interested in the localization of the oil phase by CLSM. Secondly, we imaged the two polymeric components, gelatine and arabic gum, in the

* Corresponding author. Department of Biopharmaceutics and Pharmaceutical Technology, Saarland University, Im Stadtwald, D-66123 Saarbrücken, Germany. Tel.: +49-681-302-2039; fax: +49-681-302-4677.

E-mail address: lehr@rz.uni-sb.de (C.-M. Lehr)

0939-6411/00/$ - see front matter
PII: S0939-6411(99)00063-6

capsule wall with regard to their respective distribution within the wall material. We also examined in which way an additional polymeric compound, such as casein, would affect the structure and composition of the wall material. Thereafter, we took advantage of the possibility to depict the oil phase in confocal sections and further developed this approach for the quantification of the amount of entrapped oil. This appeared to be suitable as a non-destructive method for the determination of the encapsulation rate.

2. Materials and methods

2.1. Materials

Gelatine, type A and B, with different bloom numbers was obtained from Deutsche Gelatine Fabrik Stoess and Co. (Eberbach, Germany), arabic gum was obtained from Caesar and Loretz (Hilden, Germany). Eicosapentaenoic acid ethyl ester (EPA-EE) was obtained with a purity of >96% as a gift from K.D. Pharma (Bexbach, Germany). Casein, fluorescein isothiocyanate (FITC) and rhodamine B isothiocyanate (RBITC) were purchased from Fluka (Deisenhofen, Germany); nile red, dimethyl sulfoxide (DMSO) and ethanolamine were purchased from Sigma (Deisenhofen, Germany). Glutardialdehyde was purchased from Carl Roth GmbH (Karlsruhe, Germany), Savinase® was obtained from Novo Nordisk Biotechnologie (Mainz, Germany), trypsin from Mucos Pharma GmbH (Geretsried, Germany), and neutral oil from Dynamit Nobel (Witten, Germany). Ethanol, hydrochloric and acetic acid were obtained from Merck AG (Darmstadt, Germany). All compounds were of analytical grade purity.

2.2. Methods

2.2.1. Preparation of the microparticles

A sample containing 2.5 g of gelatine was dissolved in 100 ml water at 50°C. Then the oil phase (EPA-EE or neutral oil) was emulsified in the gelatine solution (four-blade stirrer, 500–1000 rev./min, Typ RW 18, Janke and Kunkel, IKA-Werk, Staufen, Germany). The emulsion was thereafter poured into a beaker containing an aqueous solution of arabic gum (2.5%, w/v), 400 ml of water were added, the pH was lowered with hydrochloric (1N) or acetic acid (10%) to 3.0–4.3 and the system was cooled to 4°C. After sedimenting the microcapsules for 2 h, the supernatant was decanted and the particles were hardened by adding 2 × 150 ml ethanol to the sediment. Finally, the microcapsules were filtered and dried overnight until at constant weight. An alternative capsule hardening step was performed with glutardialdehyde [3] at higher volumes of oil to avoid the separation of the floating microcapsules by the decanting step. All preparation steps involving EPA-EE as oil phase were carried out under argon or CO_2 atmosphere to avoid oxidation of the unsaturated fatty acid ester.

2.2.2. Fluorescence labelling of the oil phase by nile red

Before preparing the oil-water emulsion, nile red was dissolved in the oil phase. Since nile red shows a strong susceptibility to fluorescence bleaching, a relatively high concentration of at least 1 mg/ml nile red was required.

2.2.3. Fluorescence labelling of gelatine, casein and arabic gum

The labelling protocol was based on a method published by Schreiber et al. [10]: 100 ml of the 2.5% (w/v) aqueous gelatine or casein solution were adjusted at pH 8.5 by sodium hydroxide solution (1N). The fluorescent dye, FITC or RBITC, respectively, was dissolved in DMSO at a concentration of 1 mg/ml. Subsequently, 100 μl of the dye solution were added to the polymer solution and stirred for 1 h at 40°C. The reaction was stopped by adding 50 μl thanolamine, and free FITC or RBITC was removed by ethanol extraction during the hardening step of the microcapsules. The same polymer labelling procedure was applied to the later determination of the encapsulation rate, but with a 2-fold higher FITC amount for gelatine labelling in order to obtain a continuous signal of the capsule wall. Arabic gum was labelled by following the same procedure, but at a higher pH (11.0). The labelling reaction schemes for the polymers with the fluorescence markers are shown in Fig. 1.

2.2.4. Determination of the labelling efficiency

The labelling efficiency was determined by separating the labelled polymer from the free dye with a dialysis membrane. The fluorescence of the free dye was measured using a CytoFluor™ II Microplate Fluorescence Reader from PerSeptive Biosystems (Wiesbaden, Germany). The excitation/emission wavelengths for FITC were 485/530 nm, for RBITC 530/590 nm. All labelled polymers were assayed in triplicate.

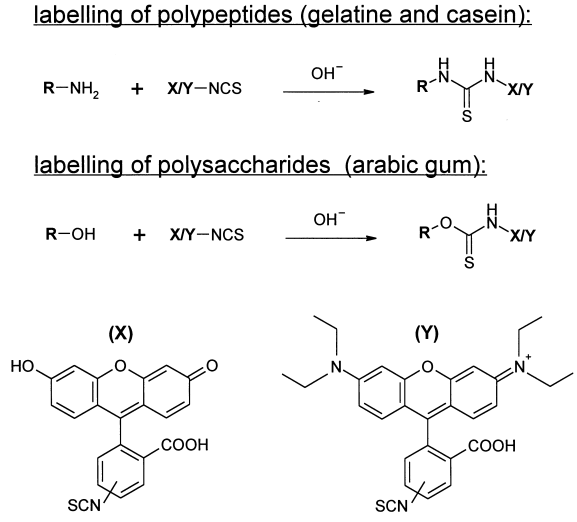

Fig. 1. Reaction schemes for the labelling procedures of the different polymers with the two fluorescence markers. X, fluoresceine isothiocyanate; and Y, rhodamine isothiocyanate.

2.2.5. Isoelectric focusing

The separation of the different types of labelled and unlabelled gelatine was performed in a Desaga DE double chamber (Heidelberg, Germany). The gel was prepared by suspending 1.4 g Biogel P-60 and 0.75 g Servalyt in 28 ml of water (pH 3–10). Two proteins were used as reference substances, BSA (IP: 4.7) and myoglobine from whale (IP: 8.3), at a concentration of 10 mg/ml. Furthermore, the free markers FITC and RBITC were applied as references. Gelatine was labelled as described above and afterwards all samples were diluted 1:1 to avoid gelation of the gelatine samples. Subsequently, 20 μl of each sample and also of the reference mix were applied to the gel. The results of the electrophoresis were analysed by staining with Coomassie blue and controlling the fluorescence signal under UV light (366 nm).

2.2.6. Confocal laser scanning microscopy

A Biorad MRC 1024 Laser Scanning Confocal Imaging System (Hemel Hempstead, UK), equipped with an argon ion laser (American Laser Corp., Salt Lake City, USA) and a Zeiss axiovert 100 microscope (Carl Zeiss, Oberkochen, Germany), was used to investigate the structure and morphology of the microcapsules. All confocal fluorescence pictures were taken with a ×40 objective (oil immersion, numeric aperture 1.30) or a ×63 objective (oil immersion, numeric aperture 1.25). The software used for the CLSM imaging was Laser Sharp MRC-1024 Version 3.1 (Bio-Rad, Deisenhofen, Germany). For imaging, a dispersion of dry microparticles in neutral oil was prepared.

2.2.6.1. Oil phase localization One fluorescence channel was used in the single red fluorescence mode at 514 nm excitation and with the filter block A1. The final pictures were composed from the mixer A (red fluorescence) and B (transmitted light) to visualize oil phase and capsule wall in the same image.

2.2.6.2. Capsule wall structure The laser was adjusted in the green/red fluorescence mode which yielded two excitation wavelengths at 488 and 514 nm. The emission filter blocks VHS/A1 and A2 were used. Green and red fluorescence images were obtained from two separate channels and a third picture from the transmitted light detector was optional.

2.2.6.3. Encapsulation Two fluorescence channels, i.e. red and green fluorescence, were composed to depict the capsule wall (FITC-labelled gelatine) by the green channel and the oil phase droplet (nile red) by the red channel. Excitation wavelengths and filter blocks were used in the same way as described above (polymer deposition). For imaging the different sections of the microcapsules two parallel *x*,*y*-planes were scanned at a distance of 5.0 or 10.0 μm by using the Z-series mode. The following computational image analysis of the CLSM pictures was performed on a personal computer and the software Scion Image [11].

2.2.7. Density measurements

Microcapsule volume was determined by a helium–air-pycnometer (Model 1302, Micromeritics Instruments corp., Norcross, USA). A steel sphere (diameter, 2.54 cm) was used for the standard volume measurements. The samples were assayed three times and weighed out directly after the volume measurements. The microcapsule density was calculated following the determination of weight and volume. All samples were analysed in triplicate.

2.2.8. Determination of encapsulation rate

2.2.8.1. Gas chromatography A sample of 100 mg of dry microcapsules was degraded enzymatically by incubation with a mixture of 5.0 ml of NH_3 solution (2 M) and 0.5 ml of Savinase® overnight in a water bath at 40°C. The microcapsule degradation was verified by light microscopy. Afterwards the EPA-EE was extracted with n-hexane and injected into the gas chromatograph (Hewlett-Packard 5880; detector: flame ionisation detection) without dilution.

2.2.8.2. Gravimetry For the determination of mass of encapsulated neutral oil we followed the same degradation and extraction procedure as described above. After extraction of the neutral oil with n-hexane and removing the solvent by evaporation, the recovered amount of neutral oil was determined gravimetrically [12]. All batches were analysed in triplicate.

3. Results and discussion

3.1. Visualization of the encapsulated phase

With the CLSM, the encapsulated oil phase could be unambiguously identified. Staining the oil phase with nile red enabled us to distinguish between encapsulated oil and other droplet-like structures, which by their shape also appeared to be oil phase, but in fact contained air (Fig. 2). This is a clear advantage of CLSM compared with conventional light microscopy. During process development or optimization, the user is able to determine quickly the localization as well as the amount of the inner oil phase qualitatively without the need to establish complex analytical procedures first.

Indeed, confocal optics are not an essential prerequisite for the qualitative identification of the encapsulated drug, which can also be performed with a non-confocal fluorescence microscope, if the drug is marked fluorescently. However, the unique advantage of CLSM is its capacity to obtain information about the three-dimensional localization of one or more fluorescently labelled compounds along (*x*,*y*,*z*) spatial dimensions.

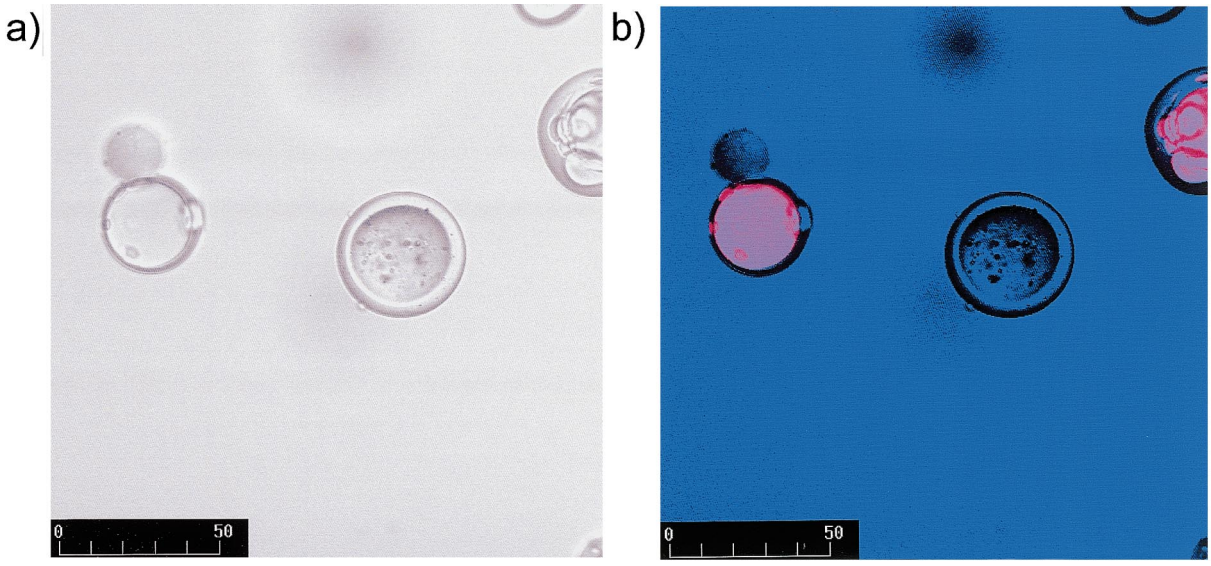

Fig. 2. Visualization of microcapsules containing a nile red stained oil phase by a light microscopy image (a) and by CLSM using the red fluorescence channel and transmitted light detection (b). The fluorescence signal allows the oil-containing and air-containing microcapsules to be unambiguously distinguished. Scale bar is shown in μm.

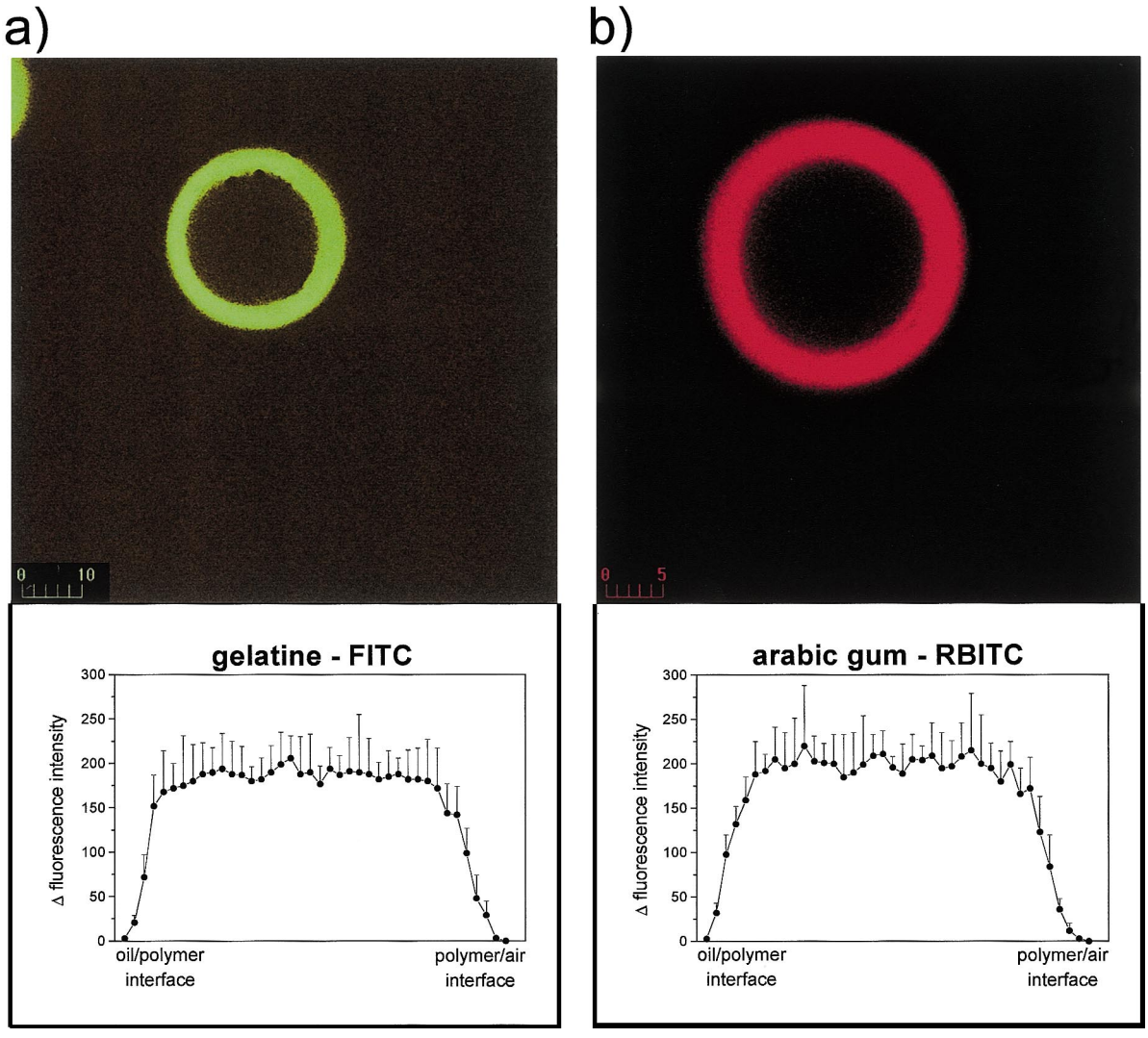

Table 1
Labelling efficiency of the fluorescence markers used with the different types of gelatine, casein and arabic gum

Polymer	Percentage of bound fluorescence marker	
	FITC	RBITC
Gelatine A bloom 100	10 ± 3	11 ± 4
Gelatine A bloom 200	18 ± 6	8 ± 3
Gelatine A bloom 300	12 ± 1	17 ± 8
Gelatine B bloom 100	9 ± 1	14 ± 2
Gelatine B bloom 200	16 ± 7	15 ± 3
Gelatine B bloom 300	10 ± 5	9 ± 2
Casein	11 ± 6	–
Arabic gum	8 ± 3	8 ± 2

It must be kept in mind, that non-fluorescent material cannot be detected by CLSM without prior fluorescence labelling. If fluorescence labelling is required for the detection of a given compound, it also has to be taken into account that fluorescence labelling may alter the physico-chemical properties of the encapsulated material. If drug and marker have similar solubility properties, mixing of marker and drug may be sufficient, and the encapsulation process and the incorporation of the drug will not be altered by the marker. But if some covalent coupling of marker and drug is required, the physico-chemical properties, especially of drugs with smaller molecular mass, may be considerably changed.

3.2. Characterization of capsule wall structure

3.2.1. Properties of the fluorescently labelled polymers

FITC and RBITC were chosen to allow the simultaneous detection in different channels. The labelling technique described by Schreiber et al. [10] was used. The concentrations of the fluorescent markers were chosen based on their stability in the laser light (photobleaching) and the labelling efficiency. In all cases the activated isothiocyanate group of the marker reacts with a nucleophil functional group of the polymer. The labelling efficiency of all polymers was between 8 and 18% (Table 1). There was a certain risk that the positively charged functional groups of gelatine, an important prerequisite for the coacervation, could be blocked after the gelatine fluorescence labelling step. However, isoelectric focusing proved no significant change of the isoelectric point for gelatine A and B, neither after labelling with FITC nor with RBITC. The fluorescence signals from the different labelled gelatines under UV light (366 nm) were consistent with the Coomassie stained bands, the signals from free markers were located elsewhere (data not shown). The labelling of gelatine obviously did not alter polymer properties relevant to the coacervation process.

The negatively charged carboxyl groups of arabic gum represent no target for the labelling step, since coupling of the markers occurs on the deprotonated hydroxyl groups of the sugar structures induced by the strong alkaline polymer solution (pH 11) [13]. Therefore, it was reasonable to assume that the coacervation behaviour of arabic gum was not significantly affected by this procedure, and fluorescently labelled arabic gum was not further characterized.

3.2.2. Deposition behaviour of gelatine and arabic gum

To examine the distribution of the polymers in the capsule wall, gelatine A or B and arabic gum were coacervated first using only one of both polymers fluorescently labelled. The structure of fluorescent markers had no influence neither on the coacervation/deposition nor on the distribution behaviour of the polymers. To characterize the polymer distribution, the fluorescence intensity across the depicted capsule wall was determined quantitatively by computational image acquisition. Twenty cross-sections through the capsule wall randomly taken from different sections of different planes were averaged to obtain a representative signal (Fig. 3). To compensate differences in wall thickness the diameters were normalized to a standard of 40 pixels. The different properties of the two types of gelatine and also their bloom number showed no influence on the distribution of gelatine in the wall material. This could be expected due to the almost negligible difference between gelatine A and B in the percentage of basic amino acids. In addition, the variation of gelatine chain length at several bloom numbers does not seem to influence the general composition of the polymer. In all experiments a homogeneous distribution for both gelatine and arabic gum was found throughout the capsule wall. In the complex coacervation process, the pH is adjusted in such a way that the gelatine is positively charged (below the isoelectric point), while arabic gum is always negative in colloidal dispersion [14]. The particle wall formation takes place based on electrostatic interaction between the polymers [14,15] and leads to a statistical distribution of the polymers throughout the wall material owing to the necessary charge equivalence of the two counterions during coacervation [14]. The observations by CLSM, showing a homogeneous distribution of the labelled polymers in all cases, are in line with this theory.

When the coacervation process was performed with gelatine-FITC and arabic gum-RBITC, it became possible to observe the polymer deposition of both polymers in the same microcapsule. It was confirmed by fluorescence spectroscopy that the two fluorescence markers did not change their fluorescence spectra after the labelling reaction (data

Fig. 3. Microcapsules prepared by complex coacervation, either prepared from gelatine-FITC and non-labelled arabic gum (a) or prepared from arabic gum-RBITC and non-labelled gelatine (b) providing that both polymers are distributed homogeneously across the capsule wall. Inserts show mean ± SD of 20 cross-sections randomly performed at the capsule wall from different sectioning planes. Scale bar is shown in μm.

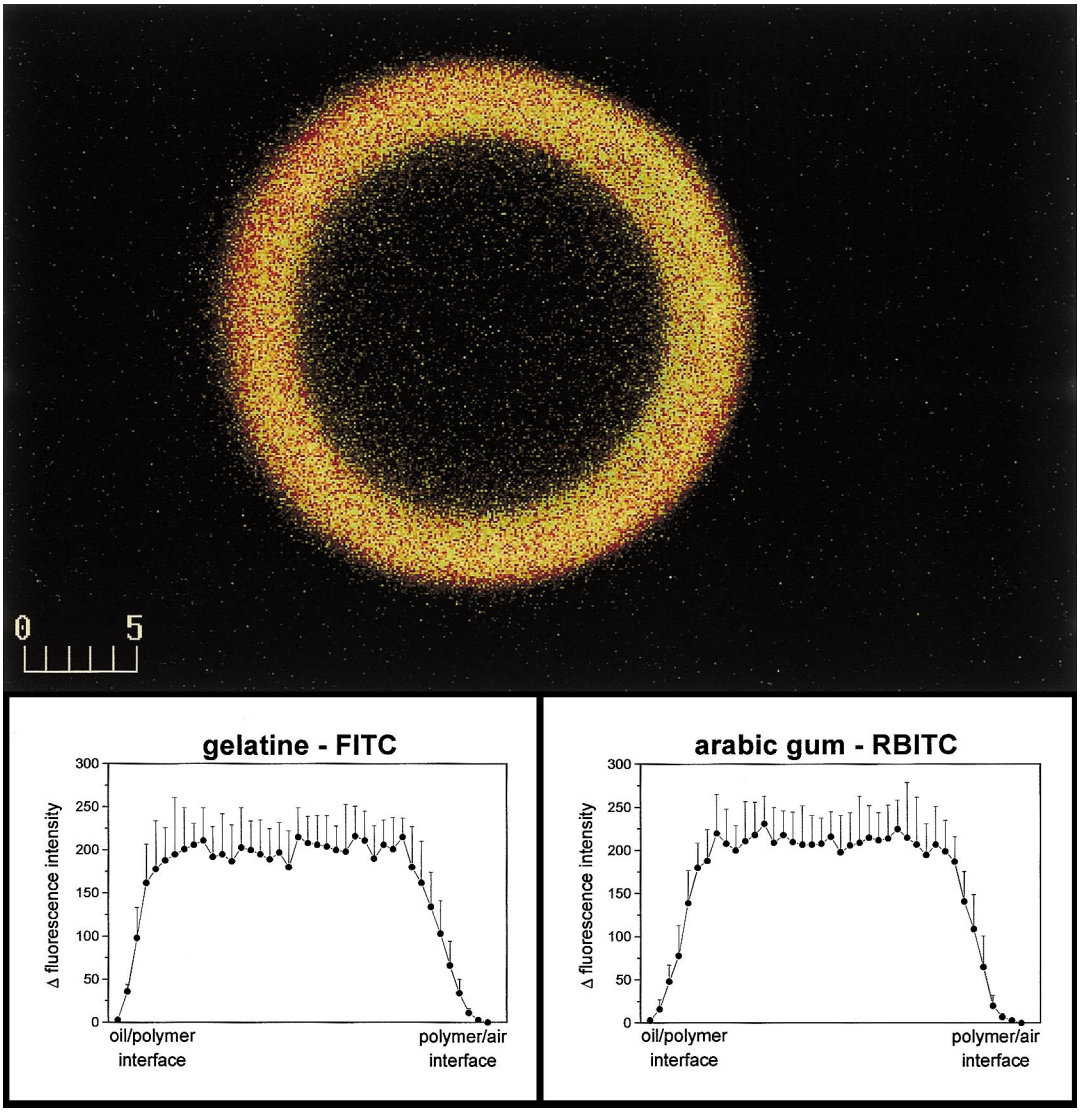
0
5
gelatine - FITC
Δ fluorescence intensity
300
250
200
150
100
50
0
oil/polymer interface
polymer/air interface
arabic gum - RBITC
Δ fluorescence intensity
300
250
200
150
100
50
0
oil/polymer interface
polymer/air interface

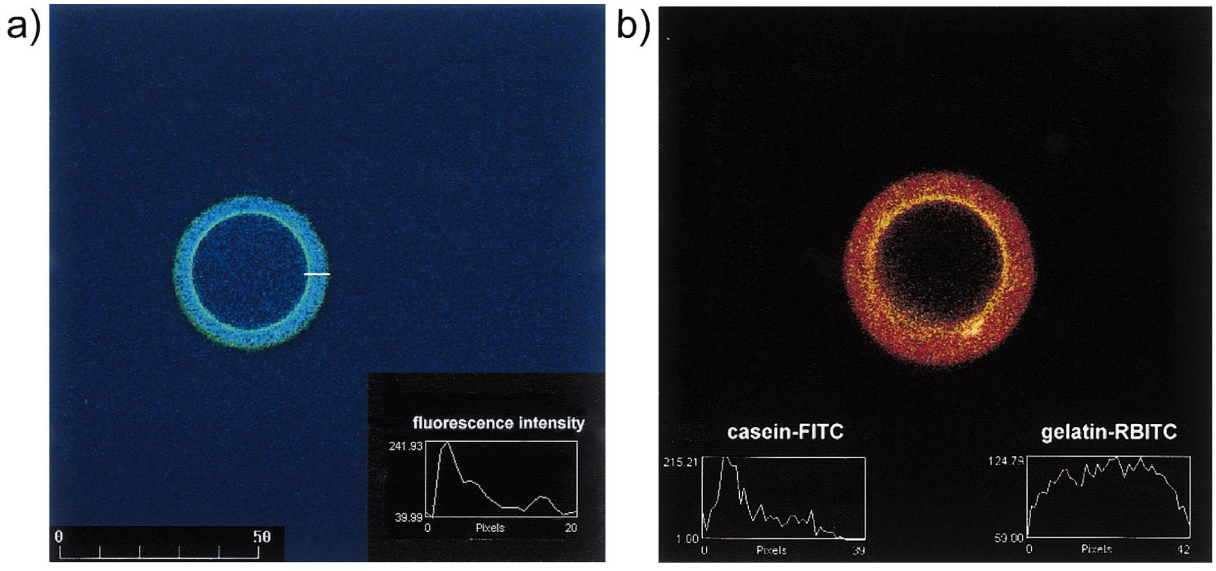
a)
fluorescence intensity
241.93
39.99
0
Pixels
20
0
50
b)
cascin-FITC
215.21
1.00
0
Pixels
gelatin-RBITC
124.79
50.00
0
Pixels
42

not shown). A homogeneous distribution of the fluorescence intensity was observed throughout the capsule wall as shown by the two inserts at the bottom of Fig. 4.

Nevertheless, an interference of both fluorescence marker signals cannot be totally excluded. The laser light at 488 nm for excitation of FITC was proved not to excite RBITC, and also no emission signal from FITC after RBITC excitation at 514 nm was found. But there remains the risk that the emitted signal from FITC provokes an excitation of RBITC and so this double labelling system cannot be used for quantitative determinations concerning the fluorescently labelled polymers. Therefore, the simultaneous visualization of two FITC and RBITC labelled polymers, respectively has to be proved by a single labelling of each polymer and the separate visualization. Using a krypton/argon laser and another set of non-interfering fluorescent probes, however, it should be possible to distinguish the different polymers quantitatively and simultaneously.

3.2.3. Deposition behaviour of casein

In order to demonstrate the potential of CLSM for visualizing the distribution of different polymers within the capsule wall, casein-FITC was added as a third component in the complex coacervation process. As shown in Fig. 5a, casein is distributed inhomogeneously throughout the capsule wall. A maximum concentration of casein was found at the oil–wall interface, decreasing towards the outer wall border. At the same time, the fluorescence signal of gelatine-RBITC still indicated a homogeneous distribution as can be seen in Fig. 5b. Similarly, the deposition behaviour of arabic gum was not influenced by the presence of casein as it was proven with arabic gum-RBITC. No influence on the casein distribution was observed while adding casein to the system before or after the emulsification step. As shown in Fig. 6 the fluorescence signal of casein-FITC decreased with lowering casein-FITC concentrations, but the pronounced gradient in the capsule wall remained. For oil-in-water emulsions with mixtures of casein and gelatine, it is known that casein is the dominant component in lowering the surface tension [16]. This seemed to be the explanation for the inhomogeneous deposition of casein.

3.3. Calculation of the encapsulation rate

Starting from the possibility of depicting the encapsulated oil phase in microcapsules we tried to develop a non-destructive method to determine the encapsulation rate by quantitative image analysis.

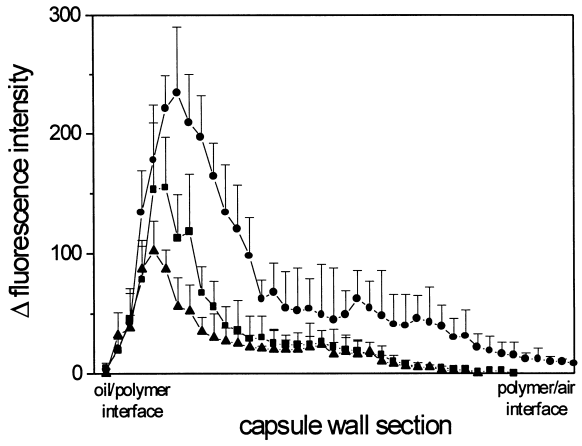

Fig. 6. Fluorescence intensity across the capsule wall for different casein concentrations (5% casein, ●; 2% casein, ■; 0.25% casein, ▲). Shown is the mean ± SD of 20 cross-sections randomly performed at the capsule wall from different sectioning planes.

This was possible because CLSM allows us to distinguish between the oil phase, the wall material and the image background. Furthermore, the quantitative analysis was facilitated by the spherical shape of both the encapsulated oil phase and the microcapsules themselves. The microcapsules were depicted in two different horizontal sections with a distance of 5 or 10 μm between the planes depending on the microcapsule size. The radius of each plane was calculated from the square pixels processed by computational image analysis. Thereafter, we determined the volume of both the oil droplet and the entire microcapsule separately according to the equations of Cavallieri [17], taking into consideration that a necessary condition for the calculations is that both depicted planes are sections from the same hemisphere. It is not required, that the encapsulated oil droplet is in the centre of the capsule. All volumes were determined by using Eq. 1, as illustrated in Fig. 7:

$$V = \frac{4\pi}{3}\left[r_2^2 + \left(\frac{r_2^2 - r_1^2 - h^2}{2h}\right)^2\right]^{3/2} \quad (1)$$

where V, is the volume of the encapsulated oil phase droplet, respectively the entire microcapsule; h, the vertical distance between the two CLSM section planes; r_1, the radius of the oil phase droplet on CLSM section 1 (r_{1O}), respectively of the microcapsule (r_{1W}); and r_2 the radius of the oil phase droplet on CLSM section 2 (r_{2O}), respectively of the microcapsule (r_{2W}).

The encapsulation ($E_{\%}$) in the microcapsules is obtained from the quotient m_{oil}/m_{caps} for the usual chemical analysis.

Fig. 4. Image of microcapsule prepared by complex coacervation including double labelling of both polymers, gelatine-FITC is represented in green, arabic gum-RBITC is represented in red. Inserts show mean ± SD of 20 cross-sections randomly performed at the capsule wall from different sectioning planes. Scale bar is shown in μm.

Fig. 5. Images of different microcapsules prepared by complex coacervation, first, with non-labelled gelatine and arabic gum containing additional casein-FITC (a), and, secondly, with gelatine-RBITC, unlabelled arabic gum and additional casein-FITC (b). Scale bar is shown in μm.

As the imaging procedure yields the volumetric ratio of oil phase and microcapsule by the quotient V_{oil}/V_{caps}, the densities of oil phase and microcapsules had to be taken into consideration. The entrapped oil amount obtained from the Eq. 2 was the basis for a later determination of the encapsulation rate.

$$E_{\%} = \frac{m_{oil}}{m_{caps}} 100 = \frac{V_{oil}}{V_{caps}} * \frac{\rho_{oil}}{\rho_{caps}} * 100 \quad (2)$$

Where $E_{\%}$ is the oil amount in the microcapsules in percent; m_{oil} the mass of the extracted oil phase; m_{caps} the mass of microcapsules used for extraction; V_{oil} the volume of the encapsulated oil phase droplet; V_{caps} the volume of the entire microcapsule; ρ_{oil} the density of the oil phase; and ρ_{caps} the density of the microcapsules.

For a measurable image (particle size range: 20–50 μm), a magnification of at least 100 times for the microscope was required since the image resolution at lower magnification was too inaccurate. It was found that for stable results of the $E_{\%}$ at least 15 randomly depicted microcapsules were needed.

In order to avoid some possible errors due to scattered light when recording a transmission light picture we decided to label both the capsule wall polymer and the encapsulated oil phase by different fluorescence labels to be recorded in separate channels. The oil phase was stained with nile red and the wall polymer gelatine labelled with FITC. Following this approach, the optical aberration was reduced to a minimum and the correct dimensions of the inner and outer

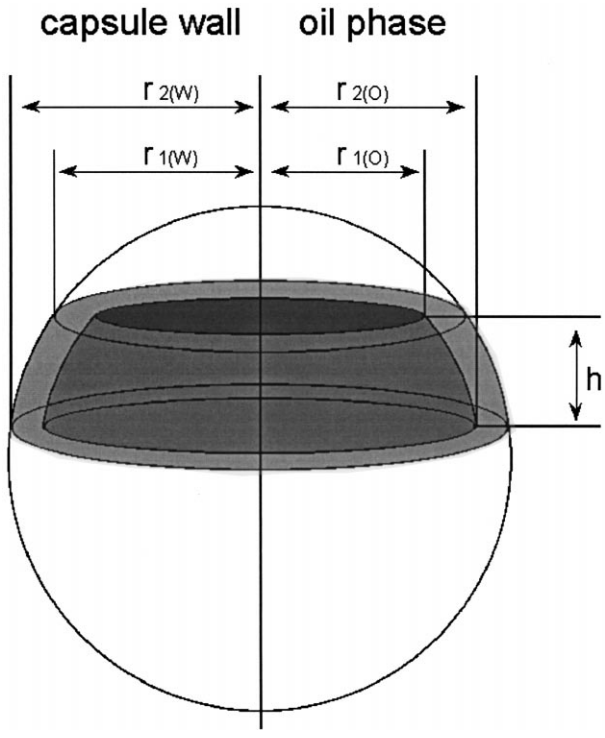

Fig. 7. Illustration for the calculations of the capsule volumes according to the Cavallieri equations.

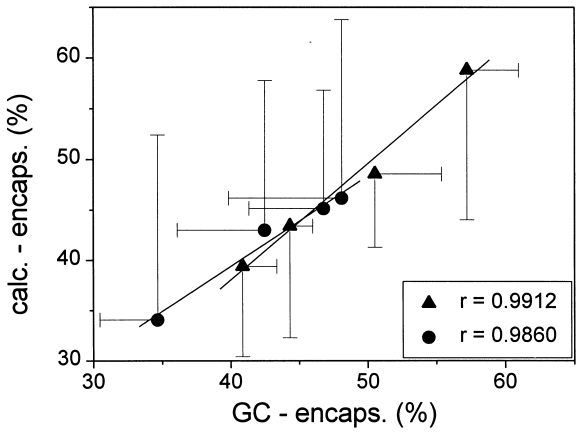

Fig. 8. Correlation between chemically determined encapsulation rate and the results from quantitative image analysis for EPA-EE (▲) and neutral oil (●) as inner oil phase (as mean ± SD for x and y). Each point represents the mean ± SD of three chemically or 15 optically analysed samples of two times four separate batches prepared under different conditions and therefore yielding different encapsulation rates.

phase of the capsule was obtained as a basis for the subsequent calculations.

Different batches of microcapsules containing EPA-EE or neutral oil as oil phase were analysed for both image analysis as well as chemical assay and an excellent correlation between the results obtained by both methods was found (Fig. 8). Correlation coefficients of 0.991 and 0.986 were calculated after linear regression and moreover the intercepts for the y-axis were not statistically different from zero as based on the 95% confidence interval.

As in all cases the fluorescence labelling procedures were observed to affect neither the capsule structure nor the process yield, the results for the determination of the encapsulation rate correlated as well as those from the $E_{\%}$ (data not shown).

Unfortunately this simple method cannot be applied immediately to also calculate the volume of non-spherical or irregularly shaped capsules or particles. In principle, however, procedures to facilitate the calculation of irregular structures have already been proposed [18], but such approaches require the acquisition and processing of much more image data and appeared to be beyond the scope of this study.

4. Conclusion

As we have shown, CLSM is a useful tool for the characterization of microcapsules. Compared to ordinary light microscopy and the technically even more demanding electron microscopy, CLSM provides additional information such as the three-dimensional localization and quantification of the encapsulated phase, as well as the polymer composition of the wall material. The encapsulated phase could be identified and exactly localized in all three spatial

dimensions. A visualization of the polymer distribution throughout the capsule wall was possible and, in particular, allowed the detection of an inhomogeneous distribution of some capsule wall polymers. By applying adequate procedures of image analysis and fluorescence labelling, CLSM may allow determination of the encapsulation rate of microcapsules without the need for any destruction, extraction and chemical assays. The results obtained by this optical method for oil-containing microcapsules correlated very well with those from chemical analysis.

Acknowledgements

We would like to thank M. Resch (Department of Physical Chemistry, Saarland University) and D. Neumann (Department of Biopharmaceutics and Pharmaceutical Technology) for their support at the laser light spectroscopy.

References

[1] B.K. Green, L. Schleicher; US Patent 2730456 (1956).
[2] B.K. Green, L. Schleicher; US Patent 2800457 (1957).
[3] L.A. Luzzi, R.J. Gerraughty, Effects of selected variables on the microencapsulation of solids, J. Pharm. Sci. 56 (1967) 634–638.
[4] C. Arneodo, J.-P. Benoit, C. Thies, Etude préliminaire de la microencapsulation d'huiles essentielles par coacervation complexe, STP Pharm. Sci. 2 (15) (1986) 303–306.
[5] R. Krumbholz, A. Lamprecht, C.-M. Lehr, U. Schäfer, N. Schirra, M. Treitz, German Patent Application 19830375.0 (1998).
[6] J.-P. Benoit, C. Thies, Microencapsulation – methods and industrial applications, in: S. Benita (Ed.), Drugs and the Pharmaceutical Sciences, 73, Marcel Dekker, New York, 1996.
[7] S. Benita, J.-P. Benoit, F. Puisieux, C. Thies, Characterization of drug-loaded poly(d,l-lactide) microspheres, J. Pharm. Sci. 73 (1984) 1721–1724.
[8] B.R. Mathews, J.R. Nixon, Surface characteristics of gelatin microcapsules by scanning electron microscopy, J. Pharm. Pharmacol. 26 (1974) 383–384.
[9] R. Bodmeier, J. McGinity, Polylactic acid microspheres containing quinidine base and quinidine sulphate prepared by the solvent evaporation technique. I. Methods and morphology, J. Microencapsul. 4 (1987) 279–288.
[10] A.B. Schreiber, J. Haimovich, Quantitative fluorometric assay for detection and characterization of Fc receptors, Methods Enzymol. 93 (1983) 147–155.
[11] Scion Image, Release Beta 3b, ©1998 Scion Corporation, 82 Worman's Mill Court, Suite H, Frederick, MA 21703, USA, http://www.scioncorp.com.
[12] M. Rabiskova, J. Song, F.O. Opawale, D.J. Burgess, The influence of surface properties on uptake of oil into complex coacervation microcapsules, J. Pharm. Pharmacol. 46 (1994) 631–635.
[13] J.A. Rendleman, Advances in chemistry, J. Am. Chem. Soc. Series (1971) 117.
[14] L.A. Luzzi, R.J. Gerraughty, Effects of selected variables on the extractability of oils from coacervate capsules, J. Pharm. Sci. 53 (1964) 429–431.
[15] H.G. Bungenberg de Jong, in: H.R. Kruyt (Ed.), Colloid Science, 2, Elsevier, Amsterdam, 1949.
[16] P.R. Mussellwhite, The surface properties of an oil-water emulsion stabilized by mixtures of casein and gelatin, J. Colloid Interface Sci. 21 (1966) 99–102.
[17] W. Gellert, H. Küstner, M. Hellwich, H. Kästner, Großes Handbuch der Mathematik, Buch und Zeit Verlagsges, Köln, Germany, 1969.
[18] L. Lucas, N. Gilbert, D. Ploton, N. Bonnet, Visualization of volume data in confocal microscopy: comparison and improvements of volume rendering methods, J. Microsc. 181 (1996) 238–252.